We are IntechOpen, the world's leading publisher of Open Access books Built by scientists, for scientists

4,800
Open access books available

122,000
International authors and editors

135M
Downloads

Our authors are among the

154
Countries delivered to

TOP 1%
most cited scientists

12.2%
Contributors from top 500 universities

CLARIVATE ANALYTICS BOOK CITATION INDEX INDEXED

WEB OF SCIENCE™

Selection of our books indexed in the Book Citation Index in Web of Science™ Core Collection (BKCI)

Interested in publishing with us?
Contact book.department@intechopen.com

Numbers displayed above are based on latest data collected.
For more information visit www.intechopen.com

Chapter 2

Design, Implementation and Modeling of Flooding Disaster-Oriented USV

Junfeng Xiong, Feng Gu, Decai Li, Yuqing He and Jianda Han

Additional information is available at the end of the chapter

http://dx.doi.org/10.5772/64305

Abstract

Although there exist some unmanned surface platforms, and parts of them have been applied in flooding disaster relief, the autonomy of these platforms is still so weak that most of them can only work under the control of operators. The primary reason is the difficulty of obtaining a dynamical model that is sufficient rich for model-based control and sufficient simple for model parameters identification. This makes them difficult to be used to achieve some high-performance autonomous control, such as robust control with respect to disturbances and unknown dynamics and trajectory tracking control in complicated and dynamical surroundings. In this chapter, a flooding disaster-oriented unmanned surface vehicle (USV) designed and implemented by Shenyang Institute of Automation, Chinese Academy of Sciences (SIA, CAS) is introduced first, including the hardware and software structures. Then, we propose a quasi-linear parameter varying (qLPV) model to approach the dynamics of the USV system. We first apply this to solve a structured modeling problem and then introduce model error to solve an unstructured modeling problem. Subsequently, the qLPV model identification results are analyzed and the superiority compared to two linear models is demonstrated. At last, extensive application experiments, including rescuing rope throwing using an automatic pneumatic and water sampling in a 2.5 m radius circle, are described in detail to show the performance of course keeping control and GPS point tracking control based on the proposed model.

Keywords: unmanned surface vehicles, quasi-linear parameter varying system, active modeling, unscented Kalman filter

1. Introduction

Floods are among the most major climate-related disasters and have resulted in substantial losses including enormous property damage and human casualties [1]. Numbers of casualties and losses could be larger in the future in response to global warming. The biggest challenge lying in rescuing operations is the low efficiency and the high risk of the rescuers, which is also a problem focused on by this work. Unmanned system is one of the solutions that replace people in the rescuing operations.

Unmanned surface vehicles (USVs), also called autonomous surface vehicles (ASVs), are often used to name the vehicles, which can run on the surface autonomously. Surface robot-assisted flood disaster rescue and inspection is a new research direction in the field of robotics. Here are some obvious advantages: (1) the smaller size allows the USVs to access to narrow and small space to get detailed information; (2) remote operation can avoid casualties of the rescuers caused by the unexpected potential dangers. After Hurricane Wilma in 2005, USVs have been used for emergency response by detecting damage to seawalls and piers, locating submerged debris, and determining safe lanes for sea navigation [2]. After the Fukushima nuclear accident in 2011, the United States and Japan have used robots to assess the damage jointly [3].

Also, in 2007, a new Trimaran unmanned surface vehicle (TUSV) as a test-bed to verify the robust motion control strategies has been designed in Shenyang Institute of Automation, Chinese Academy of Sciences (SIA, CAS) [4]. After that, in 2012, a water-jet propulsion USV equipped with different kind of sensors and ground control system has been designed and implemented in SIA to improve the performance of USV [5]. In 2015, to increase the reliability and real time of USV, the software architecture has been designed based on a real-time operating system QNX 6.5.0. Also, the selection of an appropriate platform and associated hardware as well as useful and sufficient sensors, and integrating these two entities has been taken into consideration. Modular design is adopted in the hardware and software structures to improve system scalability. The hardware structure comprises six sub-systems, including the on-board control computer sub-system, power sub-system, communication sub-system, sensor and perception sub-system, ground station sub-system, and execution sub-system. The software structure comprises six modules, the communicator module, GPS-IMU module, protocol module, tracker module, controller module, execute module, and engine module.

In general, the surface environment of flooding disasters, including fixed obstacles, floating obstacles, narrow canals, and the wind/wave/current disturbances, makes the target difficult to be inspected by an USV, because it presents a great limitation in trajectory tracking in complicated surroundings. The primary reason is the difficulty of obtaining accurate and applicable dynamical models. The hydrodynamic mechanism is very complex, and the dynamical model parameters change with Froude number $F_r = U/\sqrt{Lg}$, where U is the operating speed of USV, L is the overall length of USV (the submerged length of USV), and g is the acceleration of gravity [6]. When the Froude number is <0.5, the main fluid forces exerted on USV are the hydrostatic pressure by replacing water with respect to hydrodynamic pressure, called *displacement area*; when the Froude number is >0.5 but <1, the main fluid forces

http://dx.doi.org/10.5772/64305

exerted on USV are hydrostatic and hydrodynamic pressure, called *semi-displacement area*; when the Froude number is >1, the main forces exerted on USV are hydrodynamic pressure, called *planning area*. Since the model structure and parameters will change greatly from *displacement area* to *planning area*, there is no unified dynamics model of a surface robot.

To approximate the hydrodynamics, we propose an active quasi-linear parameter varying (qLPV) model to approach the dynamics of the USV system. The LPV model concerns linear models whose state-space representations depend on state independent parameters [7]. The qLPV model is obtained by making the varying parameter of the LPV system a function of the state [8]. To accommodate the unstructured model error, the model error is introduced into the qLPV structured model as a complementation, and with the active modeling technique, the model error online estimation is used to improve the modeling accuracy. There are many available algorithms for active model online estimation such as the extended Kalman filter (EKF) [9] and epsilon-support vector regression (ε-SVR) [10]. In this chapter, the Unscented Kalman Filter (UKF) is utilized to obtain the unstructured model error.

Finally, to show the performance of the USV systems and the modeling methods, extensive experiments have been done including rescuing rope throwing by using an automatic pneumatic, rescuing of people, air–surface robots' cooperation, environment data collection, model parameters identification, communication distance testing, and water sampling in a 2.5 m radius circle.

2. System design of flooding disaster-oriented USV

Although the parts of USVs have been applied in reality, the autonomy of these platforms is still so weak that most of them can only work under the control of operators. This makes them difficult to be used to verify some high-performance autonomous control algorithm. Thus, a new USV system equipped with different kinds of sensors and ground control system is designed and introduced in this chapter.

Modular design is adopted in hardware and software structures, and the corresponding modules will be described in detail. Every hardware module is a separate subsystem which is connected together by waterproof aviation plugs. An automatic pumping system is equipped in the USV to drain water when the water level in the hull exceeds the warning level. Similar to the hardware system, every software module is a separate processor that is connected together by shared memories. Since all processors share a single view of data, the communication between processors can be fast as memory access. When the shared memories have been created, all the processors needed to do is to map the shared memory and initialize the read/write lock of thread in shared memory struct.

2.1. Hardware design

The USV system designed and implemented in SIA, CAS is shown in **Figure 1**. Its basic parameters are provided in **Table 1**.

Figure 1. The USV platform.

Length	Width	Height	Max velocity	Payload
2800 mm	700 mm	370 mm	36 km/h	70 kg

Table 1. Performance parameters of the USV.

The material of USV is fiber-reinforced polymer (FRP) which is a composite that is suitable for structures in corrosive environment and long-span lightweight structures due to its high-strength, light-weight, and anti-corrosive qualities [11].

To improve system scalability, the hardware structure adopts modular design. The hardware structure comprises six sub-systems, including the on-board control computer sub-system, power sub-system, communication sub-system, sensor and perception sub-system, ground station sub-system, and execution sub-system.

2.1.1. On-board control computer sub-system

The on-board control computer sub-system (**Figure 2**) contains an Advantech computer UNO-2170 with 2X LAN, 4X COM, 1X 32G Compact Flash (CF), and 2X PCM-3780. The Advantech computer UNO-2170 supports QNX Neutrino Real-time Operating System (RTOS) and can be used to record the experimental data in 0.01 s. The PCM-3780 is a general purpose multiple channel counter/timer card for the PC/104 bus. It provides two 16-bit counter channels which can be used to produce the required Pulse Width Modulation (PWM) wave to control the ignition/flame switch servo, steering rudder servo, engine throttle servo, and the selector switch servo. Using the Advantech computer UNO-2170, the GPS-IMU data, and the command data from ground station sub-system can be received though two COM serial ports.

http://dx.doi.org/10.5772/64305

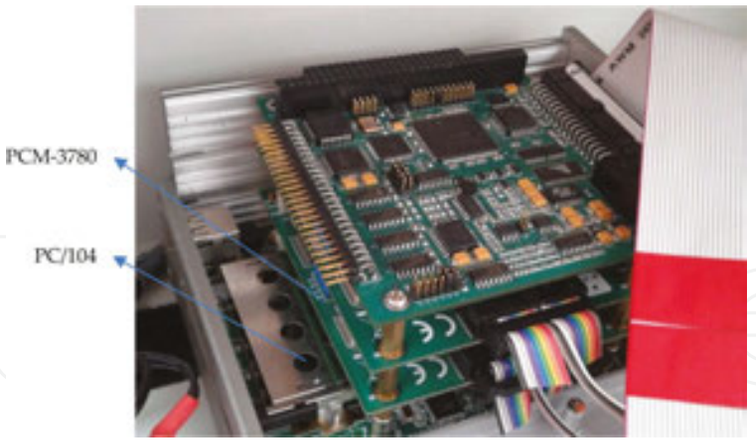

Figure 2. On-board control computer sub-system.

2.1.2. Power sub-system

The whole on-board control computer sub-system, as well as all sensors, is powered by a 12 V battery jar. Besides, considering the possibility of overvoltage at the time of switching on power, Advantech PCM-3910 DC-DC power supply module is utilized to smooth the output voltage of the battery. Moreover, the engine can generate electricity to recharge the two batteries using a battery isolator to avoid the voltage dropping when the engine is starting. The working time of the USV system is larger than 2 h.

2.1.3. Communication sub-system

The communication sub-system mainly contains a Futaba receiver, two FGR2 900 MHz industrial radios, a wireless router, and an image transmission equipment. The Futaba receiver is used to receive the signal from the Futaba remote controller in emergency case. The industrial radio in ground station sub-system is used to transform command data from ground station sub-system to on-board control sub-system, while the other industrial radio in on-board control computer sub-system is used to transform feedback data from on-board control computer sub-system to ground station sub-system. The maximum communication distance from ground station sub-system to on-board control sub-system is 20 km. The wireless router is used to connect debugging computer with UNO-2170 computer since it is not convenient to use QNX SDP on a QNX Neutrino RTOS system for self-hosted development. The image transmission equipment is used to transfer the video of the IP camera.

2.1.4. Sensor and perception sub-system

The sensor sub-system contains a GPS-IMU system (see **Table 2**), an IP camera, a sonar, and a LIDAR. The GPS-IMU is used to locate the USV and obtain some inertial states such as attitude, velocity, and acceleration. The IP camera can monitor the environment of USV both in daytime and at night since it integrates infrared and visible light sensing device. Video from the IP camera is compressed based on the standard of H.264 and is transformed into the ground

station sub-system through an image transmission equipment. The sonar and LIDAR sensors are also equipped in the USV system to detect the obstacles under and above the surface, respectively.

Specification	Value
Heading accuracy	0.2° (1 σ, base line ≥ 2 m)
Attitude accuracy	0.5° (1 σ)
Position accuracy	2 cm + 1 ppm (CEP)
Speed accuracy	0.1 m/s
Data updating rate	1 Hz/5 Hz/10 Hz/100 Hz
Gyro range	±100°/s (optional ± 300°/s)
Gyro zero offset	±100°/s

Table 2. Specification of GPS-INS (XW-GI5630).

2.1.5. Ground station sub-system

Ground station sub-system (**Figure 3**) is an important human computer interaction platform for information processing.

Figure 3. Ground station sub-system.

It is the main controller unit of the USV system except for the on-board control computer sub-system and plays an important role in assisting the operator to monitor the USV's state real-time. When the USV is in some emergency situations, the operator can take appropriate disposition to ensure the safety of the USV through the state displayed on the ground station sub-system.

http://dx.doi.org/10.5772/64305

The ground station sub-system includes a high-speed computer, two screens (one is data screen, the other is video screen), communication device and two joysticks (control the rudder angle and engine throttle of the USV system, respectively). It allows remote controller operates the USV such as ignition/flame, speed, and course keeping.

2.1.6. Execution sub-system

The execution sub-system (**Figure 4**) contains four servos: a rudder servo (used to control the rudder angle of USV), a throttle servo (used to control the throttle size), an ignition/flame servo (used to start or stop the USV), and a switch servo (used to select the ground station or the remote controller to control the USV). The four servos receive the control data from the on-board control computer sub-system or remote controller and take corresponding actions.

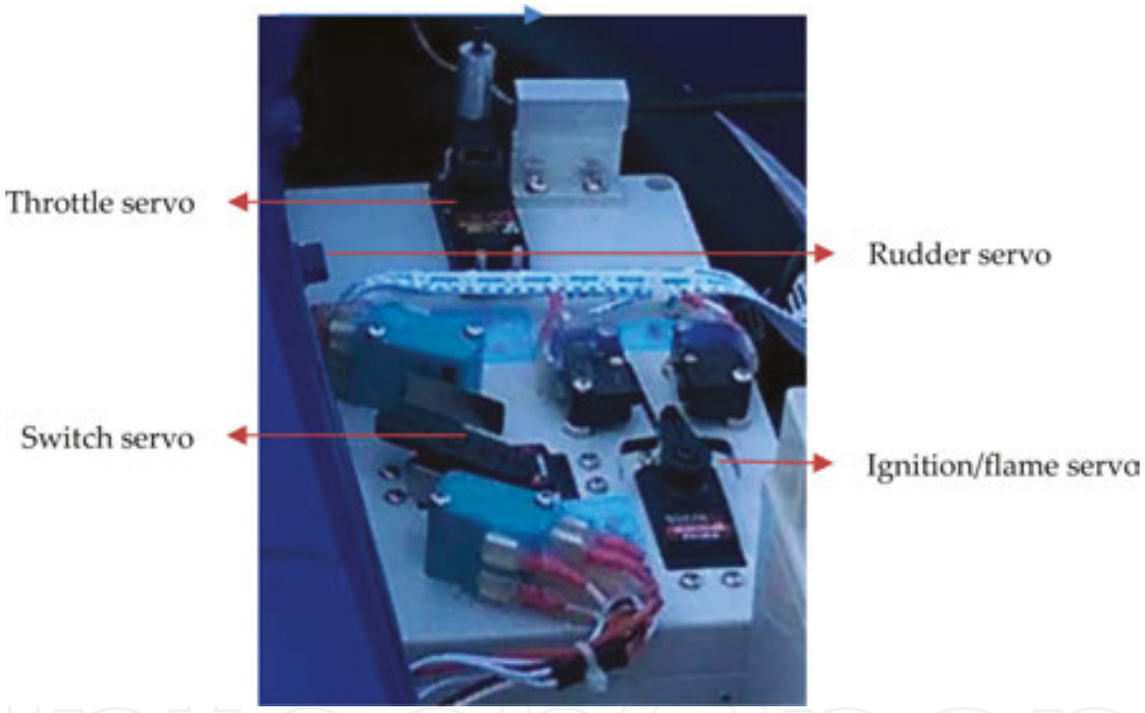

Figure 4. Execution sub-system.

2.2. Software design

Modular design is adopted in software structure. The software structure of computer control system is implemented using QNX SDP V6.5.0, a real-time operational system (RTOS), which is known as a real-time, high stable, and good portable OS. The software structure comprises six modules, the communicator module (TCP communicate and data transmit), GPS-IMU module (receive and process GPS-IMU signals), protocol module (parse the received data frame), tracker module (GPS tracking), controller module (including PID controller, ACC controller, and MPC controller), execute module (send PWM wave data to servos), and engine module (get the engine propeller speed) (**Figure 5**).

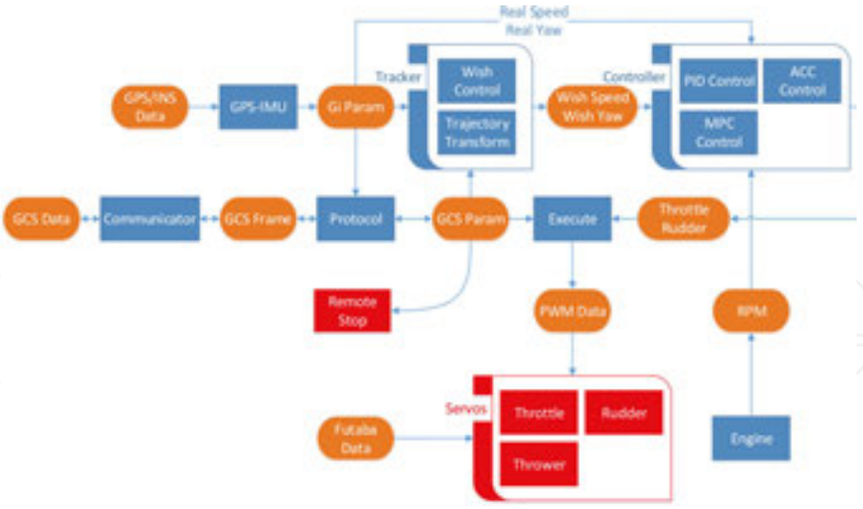

Figure 5. The software structure of USV system.

In execute module, there is an emergency sub-module that is used to stop the engine if no new data from ground station sub-system is received over 120 s. When new data from ground station sub-system are transferred to the on-board control sub-system, the execute module can generate PWM wave data to control the servos again.

In the software architecture, the key module is the controller module, which contains course keeping control, speed control, and GPS tracking control by using the measurements data from GPS-IMU module. The control period is 0.01 s.

3. USV dynamic modeling

Originally, linear models are often used owing to their simple structure, and mainly include first-order Nomoto model [12], first-order sideslip model [13], and linearized speed and steering model [14]. The Nomoto model describes the yaw dynamics between turn rate and the rudder angle input. However, when the USV's heading undergoes a small perturbation, the sideslip angle is no longer zero. To eliminate this defect in Nomoto model without considering slipping motion, one can incorporate a first-order lag model for sideslip. The sideslip model describes the sway dynamics that relates sideslip angle to turn rate. In addition to sideslip model, the linearized speed model relates the speed increment to throttle increment input. The linearized steering model relates the sideslip velocity and turn rate to rudder angle input. These models are usually effective under the assumptions: (1) the forward speed changes very slowly [15]; (2) the USV is in *displacement area* [16]. The deficiencies of the linear models are clear: (1) it presents poor performance when describing the details of the ship dynamics [17]; (2) the parameters change greatly for different speeds of the USV. This deteriorates the control performance greatly.

In addition to linear models, there are two kinds of nonlinear models, *maneuvring models* and *sea keeping models*. Maneuvring theory assumes that the USV is moving in restricted calm water.

http://dx.doi.org/10.5772/64305

Hence, the maneuvring models are derived for USV moving at positive speed U under a zero-frequency wave excitation assumption. The most famous model in maneuvring theory is the Abkowitz model [18] which adopts a nonlinear third-order truncated Taylor series expansion to approach the hydrodynamics at a nominal condition. Sea keeping theory, on the other hand, is the study of motion when there is wave excitation and the craft keeps its heading ψ and its speed U constant [18]. This introduces a dissipative force [19] known as fluid-memory effects. To estimate and identify the hydrodynamic derivatives of these nonlinear models, the forces and torque exerted on the USV need to be accurately measured. Unfortunately, this requires some strict experimental conditions that are often impossible [20].

In this section, we propose an active qLPV model to approach the hydrodynamics of USV. The advantage of the LPV model is that it is significantly simpler to be analyzed and allows the application of many linear control methods. The qLPV model is obtained by making the varying parameter of the LPV system a function of the state.

3.1. Active quasi-LPV modeling

The LPV model usually refers to the linear time-varying models that possess linear model structure but have exogenous variable $\boldsymbol{w}(t)$ dependent system matrix $\mathbf{A}$ and input matrix $\mathbf{B}$ as shown in Eq. (1) [7]. While qLPV models means that the system matrix $\mathbf{A}$ and (or) input matrix $\mathbf{B}$ depend (or depends) on some state variable $\boldsymbol{x}$ of the system itself [8], that is, the system as Eq. (1).

$$\dot{\boldsymbol{x}} = \mathbf{A}\left(\boldsymbol{w}\left(t\right)\right)\boldsymbol{x} + \mathbf{B}\left(\boldsymbol{w}\left(t\right)\right)\boldsymbol{u} \tag{1}$$

$$\dot{\boldsymbol{x}} = \mathbf{A}\left(\boldsymbol{w}\left(t\right), \boldsymbol{x}\left(t\right)\right)\boldsymbol{x} + \mathbf{B}\left(\boldsymbol{w}\left(t\right), \boldsymbol{x}\left(t\right)\right)\boldsymbol{u} \tag{2}$$

That is, qLPV models are some kinds of generation of LPV models. The reason why we select the qLPV model structure to present the USV dynamics is that the nonlinearities of an USV cannot be ignored, especially when the USV is maneuvring with quickly varying velocity and course. Therefore, to denote the strong nonlinearities, the USV system can only be transferred into the qLPV form [21]:

$$\dot{\boldsymbol{v}} = \mathbf{A}\left(\boldsymbol{v}\right)\boldsymbol{v} + \mathbf{B}\boldsymbol{u} \tag{3}$$

where $\mathbf{A}(v) = \mathbf{M}^{-1}\mathbf{N}(v)$; $\mathbf{u} = T[\sin\delta \quad \cos\delta]^{\mathrm{T}}$; $\mathbf{B} = \mathbf{M}^{-1}\begin{bmatrix} 0 & -1 & x_{\delta} \\ 1 & 0 & 0 \end{bmatrix}^{\mathrm{T}}$.

The function $\mathbf{A}(v)$ in Eq. (3) can be denoted as linear combinations of the USV's velocity, that is,

$$\mathbf{A}(\boldsymbol{v}) = \mathbf{M}^{-1}\left(\mathbf{N}_0 + \mathbf{N}_1|u| + \mathbf{N}_2|v| + \mathbf{N}_3 r + \mathbf{N}_4|r|\right) \tag{4}$$

where

$$\mathbf{N}_0 = \begin{bmatrix} X_u & 0 & 0 \\ 0 & Y_v & Y_r \\ 0 & N_v & N_r \end{bmatrix};\ \mathbf{N}_1 = \begin{bmatrix} X_{|u|u} & 0 & 0 \\ 0 & 0 & 0 \\ 0 & 0 & 0 \end{bmatrix};\ \mathbf{N}_2 = \begin{bmatrix} 0 & 0 & 0 \\ 0 & Y_{|v|v} & 0 \\ 0 & N_{|v|v} & 0 \end{bmatrix};$$

$$\mathbf{N}_3 = \begin{bmatrix} 0 & m + X_{vr} & mx_G + X_{rr} \\ -m & 0 & 0 \\ -mx_G & 0 & 0 \end{bmatrix};\ \mathbf{N}_4 = \begin{bmatrix} 0 & 0 & 0 \\ 0 & 0 & Y_{|r|r} \\ 0 & 0 & N_{|r|r} \end{bmatrix}.$$

The qLPV model structure provides two advantages: (1) its parameters can be identified by some linear algorithm resulting in a nonlinear mathematical model; and (2) mature linear control synthesis schemes can be generalized to obtain adequate performance.

To further eliminate the unstructured model error, the active modeling technique is used to account for the unstructured factors. In the preceding work, we have proposed a control architecture as following **Figure 6**.

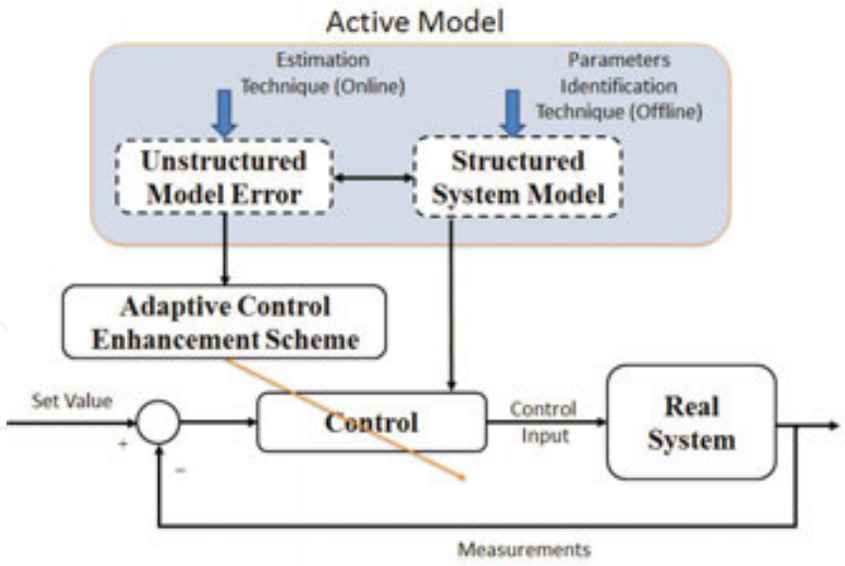

Figure 6. Active model-based control scheme.

In this architecture, the structured model can be used to design some nominal controller, while the online estimated model error is used to improve the closed loop performance of the nominal controller. To obtain the model error, we first rewrite the system Eq. (3) to follow the state-space form:

http://dx.doi.org/10.5772/64305

$$\begin{aligned} \dot{\boldsymbol{v}} &= \mathbf{A}(\boldsymbol{v})\boldsymbol{v} + \mathbf{B}\boldsymbol{u} + \Delta\boldsymbol{v} \\ \boldsymbol{z} &= \boldsymbol{v} + \boldsymbol{v}_m \end{aligned} \tag{5}$$

where v is the system state vector; $\mathbf{A}(v)v + \mathbf{B}u$ is the structured system dynamics function which is shown in Eqs. (3) and (4); Δv is the model error; z contains the measurements; and v_m contains the measurement noise.

Then, UKF algorithm is used to estimate the model error Δv using the available measurements. The UKF is an often-used nonlinear Kalman filter owing to its good performance with respect to strong nonlinearities. The main idea of the UKF algorithm is that it uses the unscented transformation (UT) to handle the nonlinear part and compute the influence of the nonlinear function on some stochastic variables. The UT provides an approach for approximating the statistics of a nonlinear transformation through a finite set of "*sigma points*":

$$\boldsymbol{z} = \boldsymbol{f}(\boldsymbol{x}) \tag{6}$$

where $\boldsymbol{f}$ is a nonlinear function and $\boldsymbol{x}$ denotes an $n \times 1$ stochastic variable with a mean of $\bar{\mathbf{x}}$ and a covariance of $\boldsymbol{P}_x$.

To calculate the propagation statistics of $\boldsymbol{x}$ through $\boldsymbol{f}$, that is, the mean $\bar{\mathbf{z}}$ and covariance $\boldsymbol{P}_z$ of the output z, the UT uses the following steps. The complete process is illustrated in **Figure 7**.

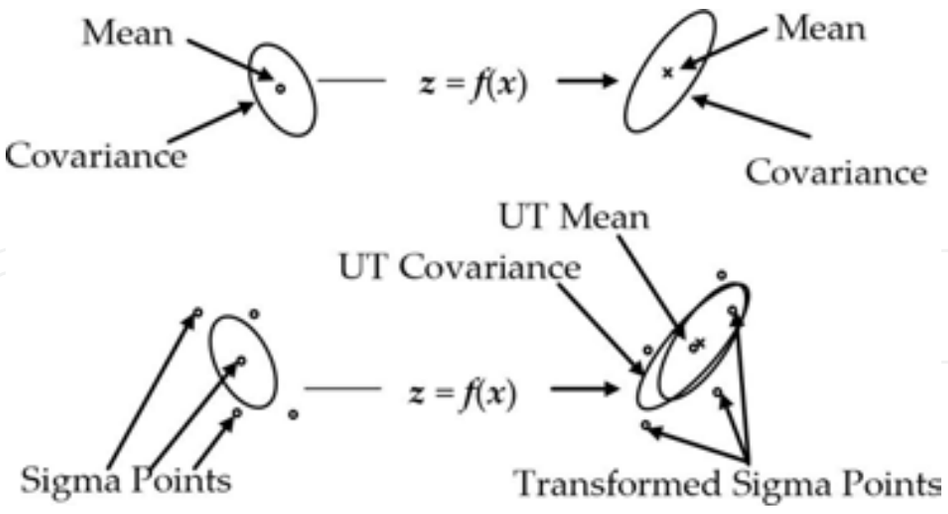

Figure 7. Unscented transformation.

The normal UKF can be deduced as follows.

UKF-I: Initialization. The measurement noise vector statistics are calculated from the initial measurement:

$$\begin{aligned}\hat{\boldsymbol{v}}_0^e &= E\left(\boldsymbol{v}_0^e\right),\\ \boldsymbol{P}_0 &= V\mathrm{ar}\left(\boldsymbol{v}_0^e\right) = E\left[\left(\boldsymbol{v}_0^e-\hat{\boldsymbol{v}}_0^e\right)\left(\boldsymbol{v}_0^e-\hat{\boldsymbol{v}}_0^e\right)^{\mathrm{T}}\right],\end{aligned} \tag{7}$$

where E[*] denotes the mean (i.e., expectation) of [*].

UKF-II: Sigma points calculation. At the kth time instant, using the kth time instant mean $\hat{\mathbf{v}}_k^e$ and covariance $\boldsymbol{P}_k$, the sigma points are defined using a Gaussian distribution.

$$\begin{aligned}\boldsymbol{\xi}_{0,k}^e &= \hat{\boldsymbol{v}}_k^e,\\ \boldsymbol{\xi}_{i,k}^e &= \hat{\boldsymbol{v}}_k^e + \left(\sqrt{(n+\lambda)\boldsymbol{P}_k}\right)_i, \quad \left(\forall i \in \{1,2,\cdots,n\}\right),\\ \boldsymbol{\xi}_{i+n,k}^e &= \hat{\boldsymbol{v}}_k^e - \left(\sqrt{(n+\lambda)\boldsymbol{P}_k}\right)_i.\end{aligned} \tag{8}$$

UKF-III: Time update. Using the sigma points, the new state is acquired:

$$\begin{aligned}\boldsymbol{\gamma}_{i,k|k-1}^e &= \boldsymbol{f}_{k-1}^e\left(\boldsymbol{\xi}_{i,k-1}^e, \boldsymbol{u}_{k-1}\right) + \boldsymbol{q}_{k-1}, \quad \left(\forall i \in \{0,1,\cdots,L\}\right),\\ \hat{\boldsymbol{v}}_{k|k-1}^e &= \sum_{i=0}^{L} W_i^m \boldsymbol{\gamma}_{i,k|k-1}^e = \sum_{i=0}^{L} W_i^m \boldsymbol{f}_{k-1}^e\left(\boldsymbol{\xi}_{i,k-1}^e, \boldsymbol{u}_{k-1}\right) + \boldsymbol{q}_{k-1},\\ \boldsymbol{P}_{k|k-1} &= \sum_{i=0}^{L} W_i^c\left(\boldsymbol{\gamma}_{i,k|k-1}^e - \hat{\boldsymbol{v}}_{k|k-1}^e\right)\left(\boldsymbol{\gamma}_{i,k|k-1}^e - \hat{\boldsymbol{v}}_{k|k-1}^e\right)^{\mathrm{T}} + \boldsymbol{Q}_{k-1}.\end{aligned} \tag{9}$$

UKF-IV: Measurements update. Similarly, using the updated state $\hat{\mathbf{v}}_{k|k-1}^e$ and $\mathbf{P}_{k|k-1}$ in ***UKF-III***, new sigma points $\boldsymbol{\xi}_{i,k|k-1}^e$ can be calculated to update the measurements.

$$\begin{aligned}\boldsymbol{\chi}_{i,k|k-1} &= \boldsymbol{h}_k^e\left(\boldsymbol{\xi}_{i,k|k-1}^e\right) + \boldsymbol{r}_k, \quad \left(\forall i \in \{0,1,\cdots,L\}\right),\\ \hat{\boldsymbol{z}}_{k|k-1} &= \sum_{\mathrm{i}=0}^{L} W_i^m \boldsymbol{\chi}_{i,k|k-1} = \sum_{\mathrm{i}=0}^{L} W_i^m \boldsymbol{h}_k^e\left(\boldsymbol{\xi}_{i,k|k-1}^e\right) + \boldsymbol{r}_k,\\ \boldsymbol{P}_{\tilde{z}_k} &= \sum_{\mathrm{i}=0}^{L} W_i^c\left(\boldsymbol{\chi}_{i,k|k-1} - \hat{\boldsymbol{z}}_{k|k-1}\right)\left(\boldsymbol{\chi}_{i,k|k-1} - \hat{\boldsymbol{z}}_{k|k-1}\right)^{\mathrm{T}} + \boldsymbol{R}_k,\\ \boldsymbol{P}_{\tilde{v}_k\tilde{z}_k} &= \sum_{\mathrm{i}=0}^{L} W_i^c\left(\boldsymbol{\xi}_{i,k|k-1}^e - \hat{\boldsymbol{v}}_{i,k|k-1}^e\right)\left(\boldsymbol{\chi}_{i,k|k-1} - \hat{\boldsymbol{z}}_{k|k-1}\right)^{\mathrm{T}}.\end{aligned} \tag{10}$$

When the new measurement z_k is obtained, the state $\mathbf{v}_k^e$ is updated:

http://dx.doi.org/10.5772/64305

$$\begin{aligned}
\boldsymbol{K}_k &= \boldsymbol{P}_{\tilde{\boldsymbol{v}}_k \tilde{\boldsymbol{z}}_k} \boldsymbol{P}_{\tilde{\boldsymbol{z}}_k}^{-1}, \\
\hat{\boldsymbol{v}}_k^e &= \hat{\boldsymbol{v}}_{k|k-1}^e + \boldsymbol{K}_k \left(\boldsymbol{z}_k - \hat{\boldsymbol{z}}_{k|k-1} \right), \\
\boldsymbol{P}_k &= \boldsymbol{P}_{k|k-1} - \boldsymbol{K}_k \boldsymbol{P}_{\tilde{\boldsymbol{z}}_k} \boldsymbol{K}_k^{\mathrm{T}},
\end{aligned} \tag{11}$$

where $\boldsymbol{Q}_k$ and $\boldsymbol{R}_k$ are the process and measurement noise covariance, respectively, which are both assumed to be known a priori. The parameter α is usually set within [0.0001, 1].

3.2. Identification results

In this section, we describe the results of two experiments: (1) full state model identification experiment; (2) active modeling enhanced qLPV model experiment. In the final, the results are analyzed and compared.

To quantitatively compare the identification errors, an index function is defined to evaluate the identification errors:

$$J_{index} = \sqrt{\frac{1}{N} \sum_{i=1}^{N} \left[x_{est}(i) - x_{ral}(i) \right]^2} \Big/ \sqrt{\frac{1}{N} \sum_{i=1}^{N} x_{ral}^2(i)} \tag{12}$$

To verify the model accuracy for different motion, experiments were conducted using a sine wave rudder angle input as shown in **Figure 8**. The quantitative comparisons are given in **Table 3**.

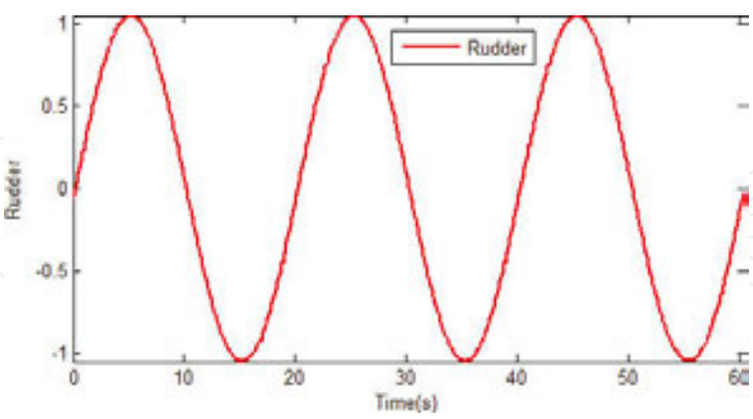

Figure 8. Sine wave rudder angle: input of the USV.

From these results, one can see that the qLPV model presents better performance for the USV system, especially for surge dynamics, for which the prediction error is <3% (no more than half of that for the two linear models). For sway dynamics, the qLPV model also provides better accuracy, but it is not as good as that for surge dynamics. This means that sway dynamics and

yaw dynamics possess stronger nonlinearity since the sway and yaw speed are usually smaller and easily influenced by external disturbances compared to surge dynamics.

	Linearized	Nomoto with sideslip	qLPV
(a) Surge dynamics	4.6%	4.6%	2.3%
(b) Sway dynamics	19.7%	17.9%	16.4%
(c) Yaw dynamics	13.7%	13.4%	13.5%

Table 3. Modeling error for sine input.

To further reduce the model mismatch's influence and improve the estimation accuracy, the active modeling scheme is used. Using an UKF algorithm, the model error of the qLPV structured model is estimated online.

The parameters of the UKF algorithm are

$$\begin{aligned} &Q = 10^{-2}\, diag\left(0,0,0,16,2,1\right), R{=}10^{-3}\, diag\left(16,2,1\right), \\ &\alpha = 1\times 10^{-3}, \beta = 2, \end{aligned} \tag{13}$$

and we use the same data as that of the full state model identification experiment, that is, the throttle was set to 30%, and the rudder angle follows a sine wave with amplitude $\pi/3$. The prediction error computed by using Eq. (12) is shown in **Table 4**. Compared to the results from the qLPV model without active modeling in **Table 3**, the model accuracy improvement is significant. The active modeling enhanced qLPV model significantly reduces the prediction errors (only one-third of that for the qLPV model). This is intended to make the USV autonomously adaptive to its internal and external uncertainties, that is, to achieve a robust tracking performance for time-varying unknown disturbances in the vehicle dynamics.

Surge	Sway	Yaw
0.8%	4.8%	4.5%

Table 4. Modeling error for active modeling enhanced qLPV model.

4. Application experiments

There are some application experiments to show the performance and application prospect of the USV system, such as rescuing rope throwing, rescuing of people, air–surface robots' cooperation, environment data collection, and water sampling. In this section, two typical

http://dx.doi.org/10.5772/64305

experiments, that is, rescuing experiment and water sampling experiment, are introduced in detail.

4.1. Rescuing experiment

The rescuing throwing experiment is aiming at searching and rescuing the trapped people (**Figure 9**). When trapped people were detected, the USV's direction would be adjusted by the ground station sub-system to launch a lifebuoy by using an automatic pneumatic. After the lifebuoy was exposed to water, it would be inflated automatically in 5 s.

a) rescuing rope throwing b) rescuing of people

Figure 9. Rescuing experiment. (a) Rescuing rope throwing and (b) rescuing of people.

The launch power is from the high-pressure (30 MPa) gas in pneumatic cylinders. The trigger servo (**Figure 10**) of the pneumatic is controlled by the PWM wave from the on-board control computer or the remote controller. The farthest distance of dumping is 150 m. Using the kayak carried by the USV, we can achieve trapped people dragging. After the trapped people reached the kayak, the ground station sub-system would send commands to USV to drag the kayak to the safe place automatically.

Figure 10. Automatic pneumatic.

4.2. Water sampling experiment

The sampling equipment is composed of four sampling bottles, a water pump and some assist mechanical devices (**Figure 11**).

Figure 11. Water sampling equipment.

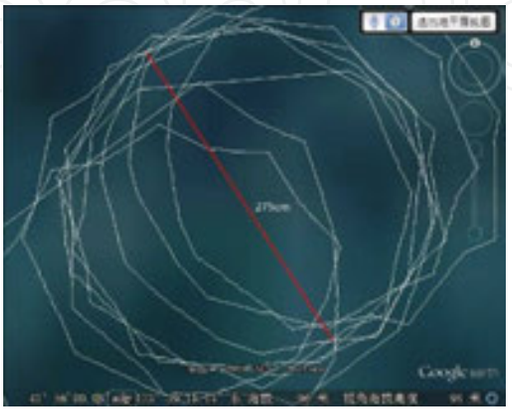

Figure 12. The minimum turning circle (radius 1.375 m).

http://dx.doi.org/10.5772/64305

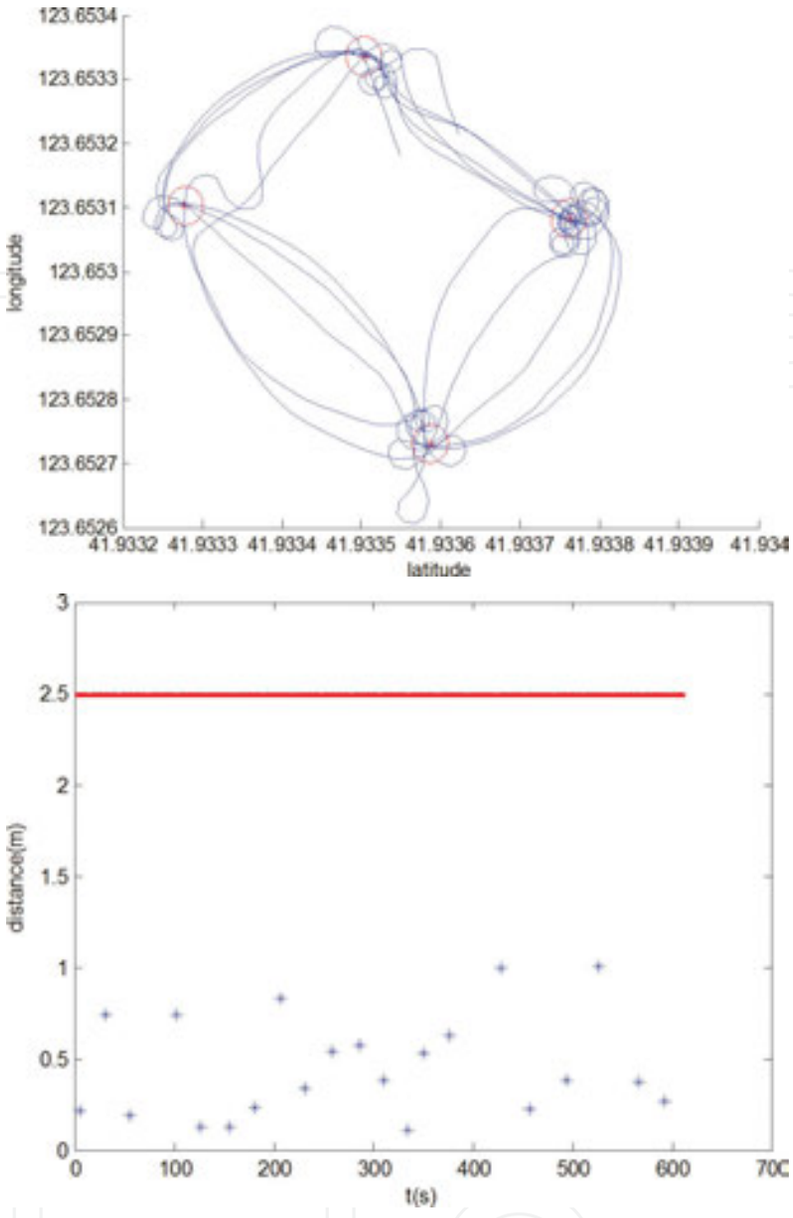

Figure 13. Four water sampling points and distance errors around the sampling points when water sampling.

First, the USV carried two sets of sampling equipment into a designed area (a 2.5 m radius circle around an GPS point). While the USV arriving at the interested point, it started to circle around the interested point at the minimum turning radius by using an GPS point tracking control algorithm (**Figure 12**). Then, the water pump protruded from the equipment and started drawing water into the bottle (each point for one bottle). After the work was done, the USV would return back automatically by using a course keeping control algorithm.

Figure 13 shows the trajectory of USV and the GPS points tracking error at four sampling points when water sampling. In the left figure, the green line represents the trajectory of USV, and the red circles are the 2.5 m radius circles around the designed sampling points. From **Figure 13**, we can see that the maximum tracking error 1.2 m, far <2.5 m.

5. Conclusions

The main concerns in this chapter is to design an real-time flooding disaster-oriented USV and construct a dynamics model for the USV system which is simple enough for model parameters identification and rich enough for motion control.

This work produced three contributions:

1. A real-time USV system adopting modular design by using different kinds of sensors and ground control system was introduced;
2. To improve model accuracy, an active qLPV nonlinear model was constructed and identified by considering both the 3-DOF rigid body dynamics and the hydrodynamics;
3. Extensive experiments were done to show the performance of the hardware and software systems.

Author details

Junfeng Xiong[1,2], Feng Gu[1], Decai Li[1], Yuqing He[1*] and Jianda Han[1]

*Address all correspondence to: heyuqing@sia.cn

1 State Key Laboratory of Robotics of Shenyang Institute of Automation, Chinese Academy of Sciences, Shenyang, China

2 University of Chinese Academy of Sciences, Beijing, China

References

[1] Hirabayashi, Y., et al., *Global flood risk under climate change*. Nature Climate Change, 2013. 3(9): p. 816–821.

[2] Murphy, R.R., et al., *Cooperative use of unmanned sea surface and micro aerial vehicles at Hurricane Wilma*. Journal of Field Robotics, 2008. 25(3): p. 164–180.

[3] Murphy, R.R., et al., *Marine heterogeneous multirobot systems at the great Eastern Japan Tsunami recovery*. Journal of Field Robotics, 2012. 29(5): p. 819–831.

[4] Qi, J., et al. *Design and implement of a trimaran unmanned surface vehicle system*. In: International Conference on Information Acquisition, 2007. ICIA'07. 2007. IEEE.

[5] Li, M., et al. *Design and implementation of a new jet-boat based unmanned surface vehicle*. In: International Conference on Automatic Control and Artificial Intelligence (ACAI 2012), 2012. IET.

[6] Faltinsen, O.M., *Hydrodynamics of high-speed marine vehicles*. 2005, Cambridge, UK: Cambridge University Press.

[7] Shamma, J.S., *An overview of LPV systems, in control of linear parameter varying systems with applications*. 2012, Springer: Berlin. p. 3–26.

[8] Raïssi, T., G. Videau, and A. Zolghadri, *Interval observer design for consistency checks of nonlinear continuous-time systems*. Automatica, 2010. 46(3): p. 518–527.

[9] Hwang, W.-Y., *Application of system identification to ship maneuvering, in Ocean Engineering*. 1980, MIT: Cambridge, MA.

[10] Zhang, X.-G. and Z.-J. Zou, *Identification of Abkowitz model for ship manoeuvring motion using ε-support vector regression*. Journal of Hydrodynamics, Series B, 2011. 23(3): p. 353–360.

[11] Peng, Q., F. Peng, and L. Ye, *Experimental study on GFRP pipes under axial compression*. Frontiers of Architecture & Civil Engineering in China, 2008. 2(1): p. 73–78.

[12] Nomoto, K., *On the steering qualities of ships*. International Shipbuilding Progress, 1957. 4(35): p. 75–82.

[13] Yu, Z., X. Bao, and K. Nonami, *Course keeping control of an autonomous boat using low cost sensors*. Journal of System Design and Dynamics, 2008. 2(1): p. 389–400.

[14] Fossen, T.I., *Guidance and control of ocean vehicles*. Vol. 199. 1994, New York: Wiley.

[15] Sarker, M.M.H., et al., *Modelling and analysis of control system for a multi-robotic system*. International Journal of Intelligent Control and Systems, 2009. 14(4): p. 221–227.

[16] Fossen, T.I., *Handbook of marine craft hydrodynamics and motion control*. 2011, New York: John Wiley & Sons.

[17] Kahveci, N.E. and P.A. Ioannou, *Adaptive steering control for uncertain ship dynamics and stability analysis*. Automatica, 2013. 49(3): p. 685–697.

[18] Abkowitz, M.A., *Lectures on ship hydrodynamics--Steering and manoeuvrability*. 1964, Hydroand Aerodynamic's Laboratory: Lyngby.

[19] Cummins, W., *The impulse response function and ship motions*. 1962, MIT: Cambridge, MA.

[20] Padilla, A., J.I. Yuz, and B. Herzer, *Continuous-time system identification of the steering dynamics of a ship on a river*. International Journal of Control, 2014. 87(7): p. 1387–1405.

[21] Xiong, J., et al., *Active quasi-LPV modeling and identification for a Water-Jet Propulsion USV: an experimental study*. IFAC-PapersOnLine, 2015. 48(28): p. 1359–1364.

IntechOpen